ORIGINAL ARTICLE

Change of Electrical and Transport Properties of Nickel Oxide by Carrier Concentration and Temperature through First-Principle Calculations

Nayem Md. Reza Shah[1] · Chang-Dong Yeo[1] · Minyeong Choi[2] · Yang-Ki Hong[2] · Jeong H. You[3]

Abstract

Nickel is typically used as one of the main components in electrical contact devices or connectors. Nickel oxide (NiO) is usually formed on the surfaces of electrodes and can negatively impact system performance by introducing electrical contact resistance. The thermal, electrical, and transport properties of NiO, as a Mott insulator or a p-type semiconductor, can be altered by operating and environmental conditions such as temperature and stress/strain by contact. In this study, we investigate the fundamental material properties of NiO through the first-principle calculations. First, we obtain and compare the lattice parameter, magnetic moment, and electronic structure for NiO via the WIEN2K simulations with four different potentials (i.e., GGA, GGA + U, LSDA, and LSDA + U). Then, using the WIEN2K simulation results with LSDA + U potential that produces a highly accurate bandgap for NiO, we calculate the electrical conductivity and electrical part of the thermal conductivity of nickel and NiO as a function of temperature and carrier concentration through the BoltzTraP simulations. Systematic simulation results revealed that the electrical conductivity relative to the relaxation time for NiO increases with the carrier concentration, while it shows a slightly decreasing trend with temperature under a fixed carrier concentration. By contrast, the electrical part of the thermal conductivity shows an increasing trend considering carrier concentration and temperature.

Highlights

1. DFT + U methods are more reliable than the DFT ones in predicting the correct bandgap of semiconductors.
2. LSDA has a good potential to obtain the magnetic moment of antiferromagnetic NiO.
3. The Seebeck coefficient of NiO is inversely proportional to carrier concentration, while its relaxation-time dependent electrical and thermal conductivities are directly proportional.

✉ Chang-Dong Yeo
changdong.yeo@ttu.edu

✉ Yang-Ki Hong
ykhong@eng.ua.edu

1 Department of Mechanical Engineering, Texas Tech University, Lubbock, TX 79409, USA

2 Department of Electrical and Computer Engineering and Material Science Ph.D. Program, The University of Alabama, Tuscaloosa, AL 35487, USA

3 Department of Mechanical Engineering, School of Engineering, University of St. Thomas, St. Paul, MN 55105, USA

1 Introduction

Nickel (Ni) is one of the most common materials used for electrodes in electrical devices such as solid oxide fuel cells, lead-free piezoelectrics, capacitive devices, and electrical connectors [1–6]. When the electrodes are exposed to an atmosphere with high temperatures during operation, nickel and other metal components on the electrodes can develop an oxidation process, which can negatively affect the performance of the system. For example, in the case of electrical contact devices such as a pin–receptacle system, if metal

🌀 Springer

oxide layers are formed on the electrode surface, then these layers can increase the electrical contact resistance (ECR), which can change the system conductivity accordingly. Electric vehicles, air fighters, and passenger aircraft are equipped with thousands of electrical connectors, and ECR is a common issue that must be addressed to acquire their sustainability under harsh operating conditions. If the ECR allowance is inappropriately controlled, then this phenomenon can lead to an electrical discontinuity or ohmic loss in the system. Therefore, the electrical and transport properties of metal oxides on the electrode surface are important parameters to obtain fundamental insights into the conductivity of systems.

A popular type of nickel is nickel oxide (NiO), which is known as an antiferromagnetic material [10], a transition metal oxide, and a p-type semiconductor [11] with a wide bandgap of 3.4–4.3 eV [12, 13]. Metal oxides can be p- or n-type depending on the type of dominant charge carriers. In p-type metal oxides such as NiO, the dominant charge carriers are the holes, while electrons are the dominant charge carriers in n-type ones such as In_2O_3 and ZnO. NiO has been used for numerous applications, such as a catalyst [14, 15], fuel cells [16], electrochromic devices [17], and gas sensors [18], due to its good chemical stability, low toxicity, low cost, and abundance. NiO is also an attractive candidate for the anode layer of solid oxide fuel cells, lithium-ion batteries, and electrochromic coatings [19].

Various computational and experimental works have been performed to investigate the thermo-electro-magnetic and transport properties of NiO. Linnera et al. [20] calculated the thermoelectric properties of NiO using the first-principle calculation. Their simulation results revealed that the Seebeck coefficient and electrical conductivity relative to the relaxation time of NiO are 900 µV/K and 2×10^{15} (Ω ms)$^{-1}$, respectively, at the temperature of 600 K, where the corresponding carrier concentration was 9×10^{16} cm^{-3}. Keem and Honig [21] measured the Seebeck coefficient of a single-crystal NiO through experiments, which produced a consistent value of 900 µV/K at 600 K. However, no corresponding carrier concentration value was included in their measurement. Another experiment by Parravano [22] controlled the hole concentration of NiO to be approximately 1×10^{21} cm^{-3}, and the resulting Seebeck coefficient was approximately 450 µV/K at 600 K. Moreover, the experimental study by Nachmann et al. [23] revealed that the thermopower of NiO was 600 µV/K at 600 K, while the electrical conductivity relative to relaxation time was 1×10^{17} (Ω ms)$^{-1}$. Considering the harsh operating conditions required for the electrical systems comprising NiO, the effects of temperature and carrier concentration on its electrical and transport properties are topics of crucial importance to sustain the conductivity of the system. Despite these outstanding achievements for NiO, quantitative discussions

on the thermal and electrical conductivity of NiO considering carrier concentration and temperature are limited. Most previous experiments and simulations for NiO have been conducted at fixed temperatures and carrier concentrations. The first-principle calculation can be affected by the type of applied potential. However, information regarding the impacts of applied potential on the calculated properties of NiO has been limited.

In this study, we investigate the thermal and electrical properties of NiO considering carrier concentration and temperature through novel computational techniques. First, the first-principle calculations are performed using the WIEN2K simulation [24–27] with four different types of potential (i.e., GGA, GGA + U, LSDA, and LSDA + U), and the band structure and density of states (DOS) of NiO are obtained. Then, the transport properties (i.e., electrical and thermal conductivity relative to relaxation time) of NiO are determined as a function of temperature and carrier concentration using the Boltzmann transport properties (BoltzTraP) simulation [28]. BoltzTraP is a simulation package based on the Boltzmann transport equation, which has widespread applications for thermoelectric research and also for obtaining transport coefficients. Using the lattice parameters, calculated energy function, wave vector (k) dependent band energies, and eigenvalues from WIEN2k or similar types of packages, BoltzTraP can calculate thermoelectric properties such as electrical and thermal conductivities and Seebeck coefficient. This study will be the first to perform a systematic evaluation of the transport properties of NiO considering carrier concentration and temperature. Therefore, the outcome of this study can contribute to the field of electrical contact devices as well as thermoelectric and semiconductor applications.

2 Computational Procedures

For the purpose of the comparative study, DFT calculations were conducted for Ni and NiO with the four potential functionals (i.e., GGA, GGA + U, LSDA, and LSDA + U). The Coulomb interaction term U = 7 eV for the GGA + U and LSDA + U potentials was applied at the 3d orbital of Ni according to the work by Li et al. [29]. As a reference, the properties of Ni were calculated to validate the computational approaches prior to the main study for NiO. The crystal structures of Ni and NiO in Fig. 1 were obtained using VESTA. NiO is an antiferromagnetic material. Thus, the magnetic moments of Ni are aligned in (111) planes, antiferromagnetically coupling with the magnetic moments in neighboring (111) planes.

First, the cutoff parameter in WIEN2K simulations was set to $R_{mt} \times K_{max} = 9$ and $G_{max} = 12.u.^{-1}$, where R_{mt} is the smallest atomic sphere radius in the unit cell, K_{max} is the
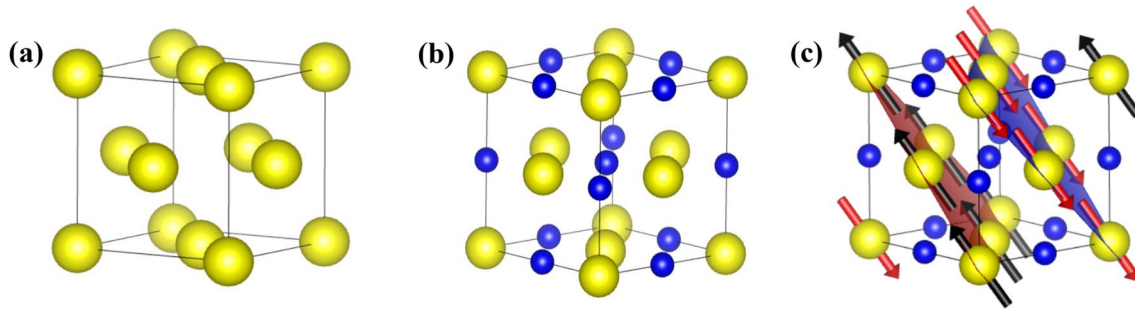
Fig. 1 Crystal structure of Ni and NiO created using the Visualization for Electronic and STructural Analysis (VESTA). **a** Ni, **b** conventional unit cell of NiO, and **c** antiferromagnetic unit cell of NiO. The yellow and blue beads are Ni and O, respectively. NiO is antiferromagnetic; therefore, the black and red arrows in **c** show the upward and downward spins, respectively

magnitude of the largest K vector, and G_{max} is the plane-wave cutoff parameter. All the calculations were obtained using 3500 k-points in the irreducible part of the Brillouin zone. A total of 3500 k-points were selected as the energy curve stabilized at 3500. The magnetic moment, DOS, and bandgap for Ni and NiO were also calculated.

Using the results of WIEN2K simulations, the electrical conductivity (σ_e/τ) and electrical part of the thermal conductivity (κ_e/τ) relative to relaxation time were then obtained through the BoltzTraP simulations. The thermal conductivity of a material depends on its free electrons and phonons. The contribution made by free electrons is known as the electrical thermal conductivity of materials, while that made by phonons is known as the phonon thermal conductivity or lattice thermal conductivity. Thermal conductivity measured in a conventional experiment yields the total thermal conductivity, which is the sum of electron and phonon contributions. Reducing the lattice thermal conductivity is crucial to enhancing the efficiency of thermoelectric materials. The electrical thermal conductivity of NiO, which is contributed by the electrons, was calculated in the current study using BoltzTraP. Therefore, this value from the BoltzTraP simulation will not match the experimental measurement, and additional computational work is required to make a complete comparison.

In BoltzTraP simulations, the wave functions were recalculated using a substantially dense k-mesh of 20,000 k-points, and the number of interpolated lattice points per k-point was set to 2. The calculation of BoltzTraP mostly depends on the wave-vector-dependent energy function. Depending on band structures or energy values considering the wave vector, the carrier concentration can be altered, which will change the resulting transport properties accordingly. Therefore, the BoltzTraP simulation used a substantially denser k-mesh than the WIEN2K simulation to obtain superior calculation results. The electrical conductivity (σ_e/τ) and thermal conductivity (κ_e/τ) of NiO can be correlated with temperature and carrier concentration based on the results of BoltzTraP simulations.

3 Results and Discussion

3.1 Lattice Constants

The lattice constants of Ni and NiO were calculated using WIEN2K simulations with the GGA, GGA + U, LSDA, and LSDA + U potentials. First, we conducted volume optimization, that is, the volume with the lowest energy value. Then, under this optimum volume, we performed the c/a ratio maximization to obtain the correct lattice parameters. The simulation results with the GGA and GGA + U potentials produced a lattice constant of 3.51–3.52 and 4.20–4.21 Å for Ni and NiO, respectively. These values agree with the experimental measurements, that is, 3.517–3.523 Å for Ni [30, 31] and 4.170–4.195 Å for NiO [32, 33]. By contrast, the lattice constant calculated from the LSDA and LSDA + U potentials was 3.42–3.43 and 4.07 Å for Ni and NiO, respectively, which are slightly smaller than the values from the GGA and GGA + U potentials. This dependency on the applied potential functional is also observed in other computational work for NiO [34–38], where the lattice constants of NiO were 4.16–4.23 and 4.04–4.18 Å with the GGA and GGA + U and the LSDA and LSDA + U potentials, respectively. Therefore, these comparative data on lattice constants could validate the WIEN2K simulations, and the resulting lattice constants were used for the following calculation of the magnetic moment and DOS.

Table 1 Magnetic moment and bandgap of NiO

Method	Magnetic moment, μ_B			Bandgap (eV)
	Ni	O	Total	
GGA	1.54	0.31	3.75	0.93
GGA + U	1.81	0.17	4.00	3.09
LSDA	0.12	0.004	0.26	0.42
LSDA + U	1.75	0.22	4.00	3.76
Reference works			3.28–4.00 [34, 38, 42–44]	3.40–4.30 [34, 38, 45–50]

3.2 Magnetic Moments

We calculated the magnetic moment of Ni and NiO using WIEN2K simulations with the GGA, GGA + U, LSDA, and LSDA + U potentials based on the lattice constants obtained in Sect. 3.1. After optimizing the lattice parameters, the structure of Ni and NiO was initialized through the selection of the potential of consideration and the specification of desired k-points. We then performed the self-consistent calculation, which produced the magnetic moments of the elements in the structures. Under the GGA, LSDA, and LSDA + U potentials, the calculated magnetic moment of Ni was 0.60–0.66 μ_B, which agrees well with the previous computational work with the GGA and LSDA [36–38] potentials and experimental measurements of around 0.59–0.66 μ_B [37, 39–41]. By contrast, the WIEN2K simulation with the GGA + U potential overestimated the magnetic moment of Ni to be 1.06 μ_B.

Next, the calculated magnetic moment of NiO is summarized in Table 1. Under the GGA, GGA + U, and LSDA + U potentials, the total magnetic moment of NiO ranged from 3.75 μ_B to 4.00 μ_B, which agrees with the previously reported values of 3.28–4.0 μ_B [34, 38, 42–44]. The LSDA potential considerably underestimated the total magnetic moment of NiO to be 0.26 μ_B. These results of calculated magnetic moments indicate that the LSDA may not be a relevant potential to analyze the magnetic property of NiO compared to the three other potentials.

3.3 DOS and Bandgap for NiO

We obtained the DOS using the WIEN2K simulations to investigate the electrically conductive characteristics of Ni and NiO. First, the DOS plots for Ni were obtained from the four different potentials, and the results were used to validate our computational approaches. As shown in Additional file 1: Fig. S1, all plots confirm that Ni is an electrically conductive material without a bandgap.

Next, Fig. 2 provides the DOS plots for NiO, where the zero in the x-axis represents the Fermi energy level.

In contrast to Ni, NiO has a semiconductor characteristic with a specific bandgap. The calculated bandgap values for NiO are summarized in Table 1. Under the GGA (Fig. 2a) and LSDA (Fig. 2b) potentials, the calculated bandgap for NiO was 0.93 and 0.42 eV, respectively, which is considerably smaller than the reported values of 3.0–4.3 eV [34, 38, 45]. However, the bandgap obtained from the DOS with the GGA + U and LSDA + U potentials produced 3.09 and 3.76 eV, respectively, which agrees with the values measured from experiments [46–50].

These results indicate that the implementation of the Coulomb interaction term U can provide a superior calculation of the NiO bandgap from the WIEN2K simulation, and the LSDA + U potential produces the most accurate bandgap value. Therefore, the WIEN2K simulation results obtained with the LSDA + U potential are applied to the BoltzTraP simulation to calculate the electrical and thermal conductivities of NiO, as described in Sect. 3.4.

3.4 Boltzmann Transport Property of NiO

3.4.1 Validation of BoltzTraP Simulation

This study aims to obtain the electrical and thermal conductivities of NiO considering temperature and carrier concentration through the BoltzTraP simulation. As explained above, we performed the BoltzTraP simulation with a substantially dense k-mesh of 20,000 k-points based on the WIEN2K simulation results for NiO under the LSDA + U potential to calculate the transport properties. First, we obtained the Seebeck coefficient and electrical and thermal conductivities for Ni considering temperature to validate the proposed computational approaches, as shown in Additional file 1: Fig. S2 and Table S1. The results showed that the Seebeck coefficient (S) of Ni decreased with temperature, as shown in Fig. S2a. The calculated Seebeck coefficient at 300 K was around − 15 μV/K, which is consistent with the previous results [51, 52]. Notably, the BoltzTraP simulation produces the electrical conductivity (σ_e) and the electrical part of the thermal (κ_e/τ) conductivity relative to relaxation time, as shown in Figs. S2b and S2c, respectively. The corresponding relaxation time should be obtained to calculate the intrinsic conductivity of Ni. We compared our results with the available experimental data (i.e., $\sigma_{electrical} = 13.3 \times 10^6$ (Ωm)$^{-1}$ at 300 K) to find the relaxation time for Ni [53]. This comparison showed that the relaxation time of Ni at 300 K is 2.77×10^{-14} s for the LSDA + U potential. Using this relaxation time value, we could calculate the thermal conductivity of Ni to be 102.22 W/m/K for the LSDA-U potential, which reasonably agrees with the reported value of 90 W/m/K [53]. Accordingly, this could validate the proposed computational approaches.
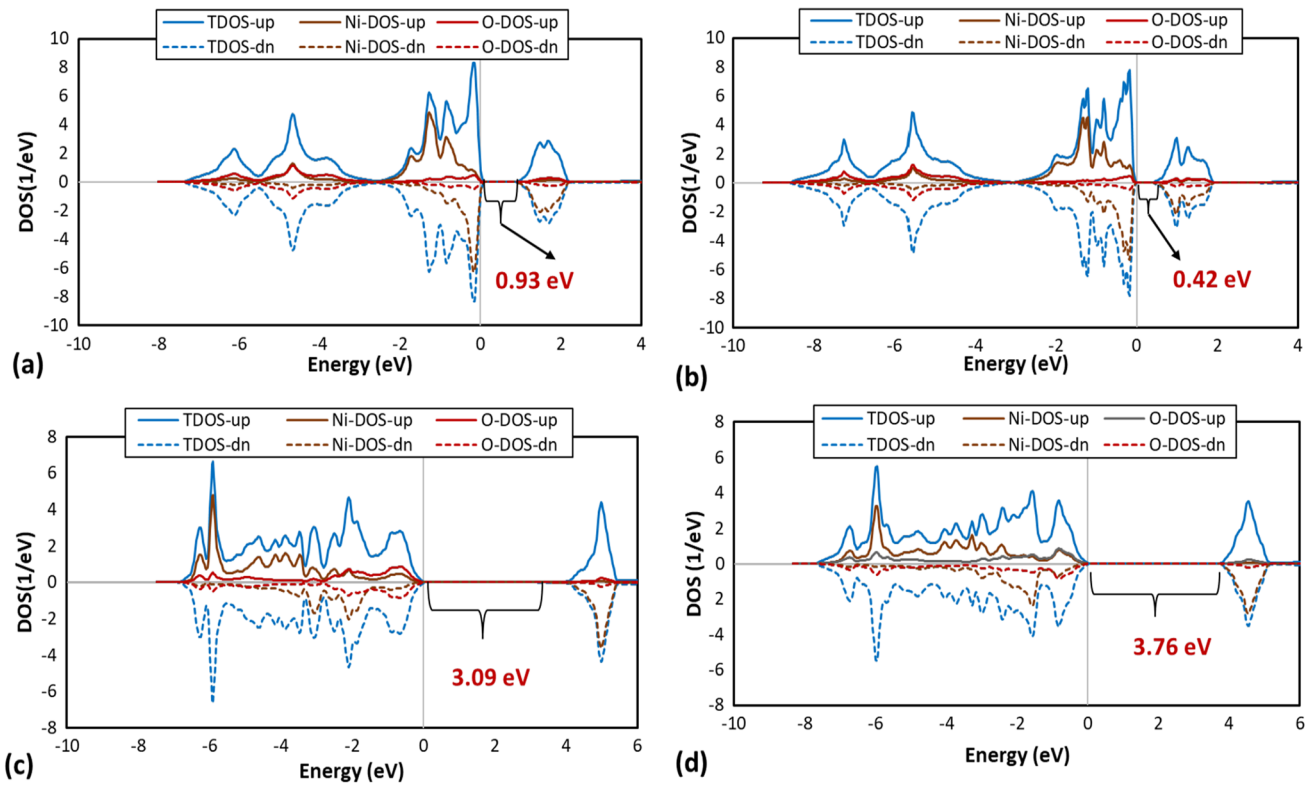
Fig. 2 DOS plots for NiO obtained from the WIEN2K simulations with **a** GGA, **b** LSDA, **c** GGA + U, and **d** LSDA + U potentials

Table 2 Calculated Seebeck coefficient and electrical conductivity of NiO compared to the previously reported values

	T (K)	Carrier concentration (cm^{-3})	S (µV/K)	σ_e/τ (Ω ms)$^{-1}$
Our calculations	600 K	9.0×10^{16}	942.17	2.36×10^{15}
	600 K	2.18×10^{18}	675.15	0.50×10^{17}
Linnera et al. [20]	600 K	9.0×10^{16}	900.00	2.00×10^{15}
Keem and Honig [21]	600 K	N/A	900	N/A
Nachman et al. [23]	600 K	2.18×10^{18} (measured at 300 K)	600	1.00×10^{17}

Next, we calculated the thermoelectrical properties of NiO considering temperature and carrier concentration using the same computational approaches performed for Ni.

First, considering some previously published work on the Seebeck coefficient (S) and electrical conductivity/relaxation time (σ_e/τ) for NiO at a fixed temperature and carrier concentration, we compared our calculations with previously reported values. This comparison is summarized in Table 2.

Based on our BoltzTraP simulations with the LSDA + U potential, when the temperature and carrier concentration were fixed to 600 K and 9.0×10^{16} cm^{-3}, respectively, the calculated Seebeck coefficient and electrical conductivity (σ_e/τ) relative to relaxation time were $S = 942.17$ µV/K and $\sigma_e/\tau = 2.36 \times 10^{15}$ (Ω ms)$^{-1}$, respectively. This result agrees with previous computational and experimental works [20, 21]. Linnera et al. [20] computed the Seebeck coefficient and electrical conductivity (σ_e/τ) relative to relaxation time for NiO at the same temperature and carrier concentration, which were 900.00 µV/K and 2.00×10^{15} (Ω ms)$^{-1}$, respectively. The experimental work by Keem and Honig [21] measured the Seebeck coefficient for NiO to be 900 µV/K at 600 K. In addition, we calculated S and σ_e/τ values for NiO using the carrier concentration of 2.18×10^{18} cm^{-3} with the fixed temperature of 600 K, which produced $S = 675.15$ µV/K and $\sigma_e/\tau = 0.5 \times 10^{17}$ (Ω ms)$^{-1}$. The experimental measurement by Nachman et al. [23] calculated the properties of NiO using the same carrier concentration of 2.18×10^{18} cm^{-3}, which provided $S = 600$ µV/K and $\sigma_e/\tau = 1.0 \times 10^{17}$ (Ω ms)$^{-1}$. Comparing our simulations to the experimental measurements, our calculated σ_e/τ value
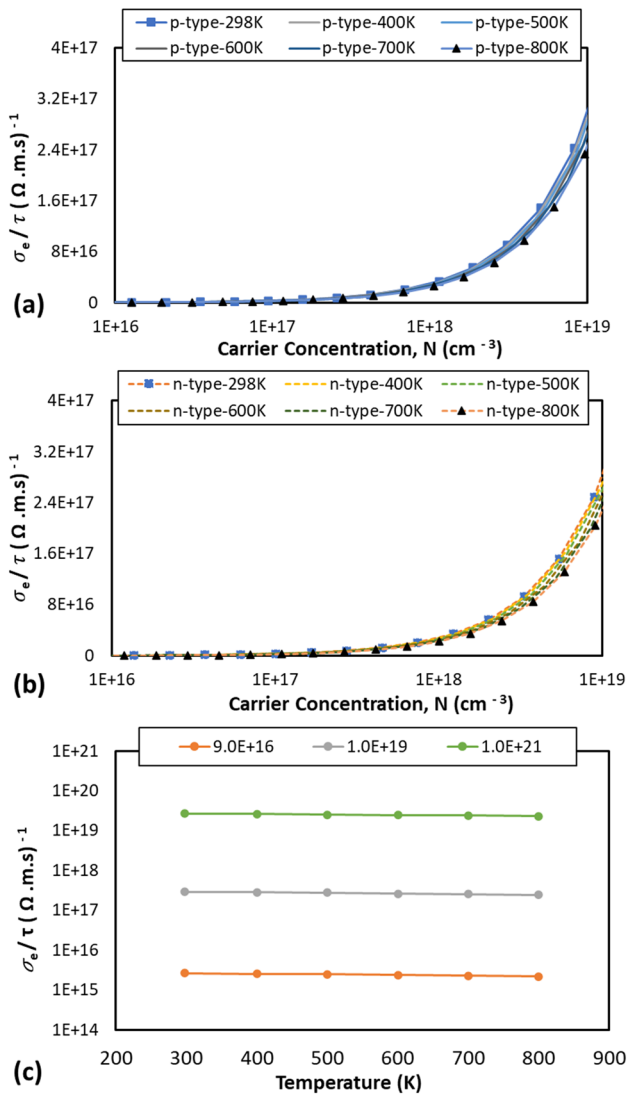
Fig. 3 Electrical conductivity relative to relaxation time (σ_e/τ) for NiO: **a**, **b** are the changes of σ_e/τ considering carrier concentration for p- and for n-type carriers, respectively. **c** is the change of σ_e/τ considering temperature

Fig. 4 Thermal conductivity relative to relaxation time (κ_e/τ) for NiO: **a**, **b** are the changes of κ_e/τ considering carrier concentration for p- and for n-type carriers, respectively. **c** is the change of κ_e/τ considering temperature

is lower than the experiment despite reasonable matching of the measured S value. Notably, the temperature in our simulations was fixed at 600 K for all procedures. However, in the experiment, Nachman et al. [23] first obtained the carrier concentration at 300 K and then measured the conductivity at 600 K. This finding indicates that the actual carrier concentration in their experiment at 600 K would be different from the value obtained at 300 K, which would be the reason for the difference between our calculations and their experimental measurements. Therefore, we can validate the computational approaches based on the aforementioned comparative data to calculate the thermoelectrical properties of NiO considering temperature and carrier concentration.
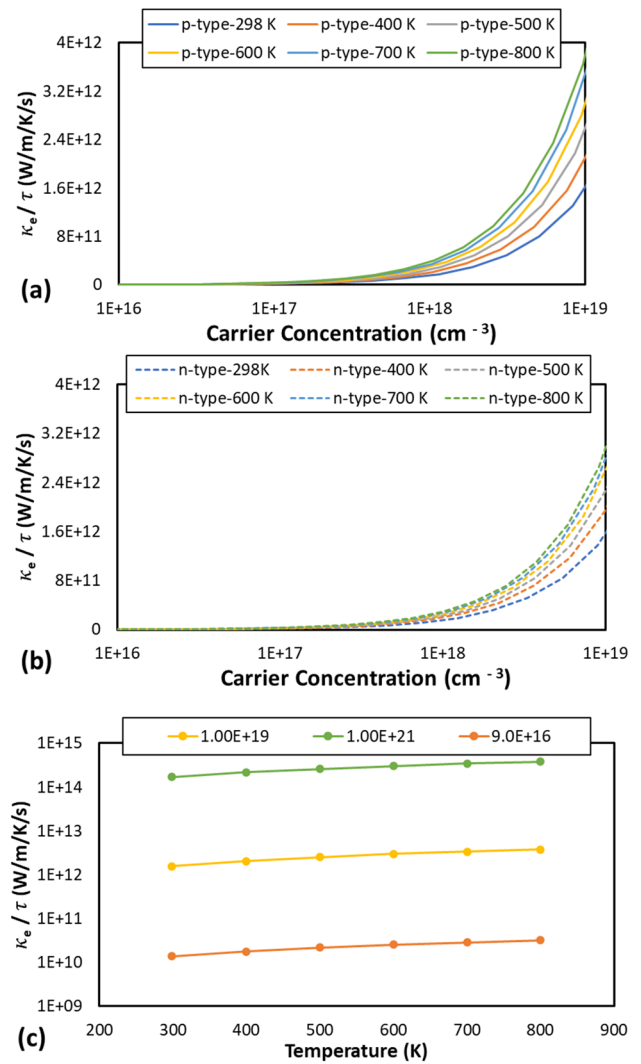
3.4.2 Electrical and Thermal Conductivities of NiO Considering Temperature and Carrier Concentration

Using the computational procedures described above, we calculated the electrical (σ_e/τ) and thermal conductivity (κ_e/τ) relative to relaxation time for NiO considering temperature and carrier concentration. First, Fig. 3 shows the change of σ_e/τ considering carrier concentration, which was obtained at different temperatures ranging from 298 to 800 K. We found that the σ_e/τ value of NiO for p-type (Fig. 3a) and n-type (Fig. 3b) carriers increases with the carrier concentration. We plotted the trend of σ_e/τ with temperature at fixed carrier concentration numbers of 9.0×10^{16}, 1.0×10^{19}, and 1.0×10^{21} cm^{-3} to evaluate the effects of

temperature on the electrical conductivity, as shown in Fig. 3c. The results revealed that the σ_e/τ value of NiO is insignificantly affected by the temperature within the tested range of temperatures. Next, Fig. 4 provides the calculated κ_e/τ value for NiO considering carrier concentration, which was obtained at different temperatures ranging from 298 to 800 K. Similarly, the κ_e/τ values for p-type (Fig. 4a) and n-type (Fig. 4b) carriers increased with the carrier concentration. Compared to the results of σ_e/τ in Fig. 3c, the thermal conductivity (κ_e/τ) relative to relaxation time demonstrated an increasing trend with the temperature.

The relationship between the electrical and thermal conductivities of a material and temperature is dependent upon its type. Metals typically have several available carriers that can move freely. Therefore, if the material temperature increases, then the carriers will obtain additional energy and move with high velocity accordingly. Consequently, additional collisions will occur between the carriers, which will increase resistivity (or decrease conductivity). Semiconductors do not have free carriers at 0 K because valence electrons are tightly bonded. When the temperature of semiconductors increases, the covalent bonds in the crystal structure start to break due to the increased energy, which generates free electrons and holes. Therefore, nearby electrons attempt to fill up the empty space (holes). Through this mechanism, electrons can move and flow, thereby increasing the conductivity of a semiconductor. As a semiconductor, the conductivity of NiO is expected to increase with temperature. Based on our calculations in Figs. 3c and 4c, the thermal conductivity relative to relaxation time (κ_e/τ) slightly increased with the temperature, but the electrical conductivity relative to relaxation time (σ_e/τ) was only slightly affected by the temperature. This weak relationship with the temperature might be attributed to the temperature dependency of the relaxation time value for NiO. The calculated conductivity is a relative value to the relaxation time (σ_e/τ). Thus, the relaxation time value for NiO should be determined as a function of temperature, (T), to obtain the exact relationship between conductivity and temperature. The relaxation time of semiconductors decreases with temperature [54–57]. Therefore, the τ value for NiO becomes small at high temperatures, which can provide a clear relationship between the calculated conductivity value and the applied temperature accordingly, similar to increasing conductivity with temperature.

4 Conclusion

The magnetic, electrical, and transport properties of NiO were calculated using the framework of density functional and Boltzmann transport theories. The lattice constants, magnetic properties, and DOS of NiO were calculated through WIEN2K simulations with four different potentials (i.e., GGA, GGA + U, LSDA, and LSDA + U). The lattice constants of NiO obtained from GGA and GGA + U potentials were close to the experimental measurements, while the simulations with LSDA and LSDA + U potentials produced small values. The magnetic moment of NiO calculated from GGA + U and LSDA + U potentials matched well with the experimental measurements, but the results with GGA and LSDA potentials underestimated it. The DOS and bandgap for NiO were best described with the LSDA + U potential compared to the three other potentials. Therefore, using the results of the WIEN2K simulation with LSDA + U potential, the BoltzTraP simulations were performed to determine the electrical conductivity (σ_e/τ) and electrical part of the thermal conductivity (κ_e/τ) of NiO considering temperature and carrier concentration. The results revealed that electrical conductivity relative to relaxation time (σ_e/τ) increased with the carrier concentration but was not significantly changed with temperature under a fixed carrier concentration. The electrical part of the thermal conductivity relative to the relaxation time (κ_e/τ) showed an increasing trend considering carrier concentration and temperature.

This study quantitatively evaluates the transport properties of NiO considering carrier concentration and temperature. The impact of strain is also crucial because current and future devices made of NiO are required to operate under harsh temperatures and stress. Studying the individual and coupled effects of temperature and strain on the properties of NiO through novel experimental and computational techniques is necessary to further contribute to the thermoelectric and semiconductor sectors.

Declarations

References

1. Müller AC, Herbstritt D, Ivers-Tiffée E (2002) Development of a multilayer anode for solid oxide fuel cells. Solid State Ionics 152:537–542

2. Wang Z, Qian J, Cao J, Wang S, Wen T (2007) A study of multilayer tape casting method for anode-supported planar type solid oxide fuel cells (SOFCs). J Alloys Compd 437(1–2):264–268

3. Randall CA, Kelnberger A, Yang GY, Eitel RE, Shrout TR (2005) High strain piezoelectric multilayer actuators—a material science and engineering challenge. J Electroceram 14(3):177–191

4. Kobayashi K, Doshida Y, Mizuno Y, Randall CA (2012) A route forwards to narrow the performance gap between PZT and lead-free piezoelectric ceramic with low oxygen partial pressure processed $(Na_{0.5}K_{0.5})$ NbO$_3$. J Am Ceram Soc 95(9):2928–2933

5. Kawada S, Kimura M, Higuchi Y, Takagi H (2009) (K, Na) NbO$_3$-based multilayer piezoelectric ceramics with nickel inner electrodes. Appl Phys Express 2(11):111401

6. Heidary DSB, Randall CA (2017) Preserving nickel electrode conductivity during sintering process using lithium carbonate coatings. J Alloys Compd 695:1448–1454

7. https://www.schleich.com/en/hotspot/electric-vehicles-automotive-hybrid-en/

8. https://www.af.mil/

9. https://www.fclane.com/news/aerospace-and-military-connectors-criteria-buyers

10. Fujii E, Tomozawa A, Torii HTH, Takayama RTR (1996) Preferred orientations of NiO films prepared by plasma-enhanced metalorganic chemical vapor deposition. Jpn J Appl Phys 35(3A):L328

11. Sato H, Minami T, Takata S, Yamada T (1993) Transparent conducting p-type NiO thin films prepared by magnetron sputtering. Thin Solid Films 236(1–2):27–31

12. Sasi B, Gopchandran KG, Manoj PK, Koshy P, Prabhakara Rao P, Vaidyan VK (2002) Preparation of transparent and semiconducting NiO films. Vacuum 68(2):149–154

13. Hassan AJ (2014) Study of optical and electrical properties of nickel oxide (NiO) thin films deposited by using a spray pyrolysis technique. J Mod Phys 5(18):2184

14. Roslik AK, Konev VN, Maltsev AM (1995) Some aspects of the mechanism of high-temperature oxidation of nickel in SO$_2$. Oxid Met 43(1):59–82

15. Roslik AK, Konev VN, Maltsev AM (1995) Sulfide-forming features during oxidation of predeformed nickel in SO$_2$. Oxid Met 43(1):83–95

16. Chen X, Wu NJ, Smith L, Ignatiev A (2004) Thin-film heterostructure solid oxide fuel cells. Appl Phys Lett 84(14):2700–2702

17. Ahn K-S, Nah Y-C, Sung Y-E (2002) Surface morphological, microstructural, and electrochromic properties of short-range ordered and crystalline nickel oxide thin films. Appl Surf Sci 199(1–4):259–269

18. Fasaki I, Giannoudakos A, Stamataki M, Kompitsas M, György E, Mihailescu IN, Roubani-Kalantzopoulou F, Lagoyannis A, Harissopulos S (2008) Nickel oxide thin films synthesized by reactive pulsed laser deposition: characterization and application to hydrogen sensing. Appl Phys A 91(3):487–492

19. Danjumma SG, Abubakar Y, Suleiman S (2019) Nickel oxide (NiO) devices and applications: a review. Int J Eng Res Technol 8:12–21

20. Linnera J, Sansone G, Maschio L, Karttunen AJ (2018) Thermoelectric properties of p-type Cu$_2$O, CuO, and NiO from hybrid density functional theory. J Phys Chem C 122(27):15180–15189

21. Keem JE, Honig JM (1978) Selected electrical and thermal properties of undoped nickel oxide. Cindas Report 52

22. Parravano G (1955) Thermoelectric behavior of nickel oxide. J Chem Phys 23(1):5–10

23. Nachman M, Cojocaru LN, Ribco LV (1965) Electrical properties of non-stoichiometric nickel oxide. Physica Status Solidi (B) 8(3):773–783

24. Blaha P, Schwarz K, Tran F, Laskowski R, Madsen GK, Marks LD (2020) WIEN2k: an APW+ lo program for calculating the properties of solids. J Chem Phys 152(7):074101

25. Hohenberg P, Kohn W (1964) Inhomogeneous electron gas. Phys Rev 136(3B):B864

26. Kohn W, Sham LJ (1965) Self-consistent equations including exchange and correlation effects. Phys Rev 140(4A):A1133

27. Ziesche P, Kurth S, Perdew JP (1998) Density functionals from LDA to GGA. Comput Mater Sci 11(2):122–127

28. Madsen GK, Singh DJ (2006) BoltzTraP. A code for calculating band-structure dependent quantities. Comput Phys Commun 175(1):67–71

29. Li RS, Xin DQ, Huang SQ, Wang ZJ, Huang L, Zhou XH (2018) A full potential all-electron calculation on electronic structure of NiO. Chin J Phys 56(6):2829–2836

30. Owen EA, Yates EL, Sully AH (1937) Proceedings of the Physical Society (1926–1948) 49(3):315

31. Bandyopadhyay J, Gupta KP (1977) Low temperature lattice parameter of nickel and some nickel-cobalt alloys and Grüneisen parameter of nickel. Cryogenics 17(6):345–347

32. Hotovy I, Huran J, Spiess L (2004) Characterization of sputtered NiO films using XRD and AFM. J Mater Sci 39(7):2609–2612

33. Rohrbach A, Hafner J, Kresse G (2004) Molecular adsorption on the surface of strongly correlated transition-metal oxides: a case study for CO/NiO (100). Phys Rev B 69(7):075413

34. Cai T, Han H, Yu Y, Gao T, Du J, Hao L (2009) Study on the ground state of NiO: the LSDA (GGA)+ U method. Physica B 404(1):89–94

35. Soman AK, Kuppusami P, Rabel AM (2017) Electrical conductivity of NiO-gadolinia doped ceria anode material for intermediate temperature solid oxide fuel cells. In: Nano hybrids and composites, vol 17, pp 224–236. Trans Tech Publications Ltd

36. Bredow T, Gerson AR (2000) Effect of exchange and correlation on bulk properties of MgO, NiO, and CoO. Phys Rev B 61(8):5194

37. Fritsche L, Koller J (2003) Potentials in density functional theory and the importance of sum rules. J Solid State Chem 176(2):652–670

38. Cinquini F, Giordano L, Pacchioni G, Ferrari AM, Pisani C, Roetti C (2006) Electronic structure of NiO/Ag (100) thin films from DFT+ U and hybrid functional DFT approaches. Phys Rev B 74(16):165403

39. Mohammed YS, Yan Y, Wang H, Li K, Du X (2010) Stability of ferromagnetism in Fe Co, and ni metals under high pressure with GGA and GGA+ U. J Magn Magn Mater 322(6):653–657

40. Chioncel L, Vitos L, Abrikosov IA, Kollar J, Katsnelson MI, Lichtenstein AI (2003) Ab initio electronic structure calculations of correlated systems: an EMTO-DMFT approach. Phys Rev B 67(23):235106

41. Huang LF, Rondinelli JM (2017) Electrochemical phase diagrams of Ni from ab initio simulations: role of exchange interactions on accuracy. J Phys Condens Matter 29(47):475501

42. Fender BEF, Jacobson AJ, Wedgwood FA (1968) Covalency parameters in MnO, α-MnS, and NiO. J Chem Phys 48(3):990–994

43. Barin I, Platzki G (1989) Thermochemical data of pure substances, vol 304, no. 334. VCh, Weinheim, p 1117

44. Hüfner S, Osterwalder J, Riesterer T, Hulliger F (1984) Photoemission and inverse photoemission spectroscopy of NiO. Solid State Commun 52(9):793–796

45. Sawatzky GA, Allen JW (1984) Magnitude and origin of the band gap in NiO. Phys Rev Lett 53(24):2339

46. Irwin MD, Buchholz DB, Hains AW, Chang RP, Marks TJ (2008) p-Type semiconducting nickel oxide as an efficiency-enhancing anode interfacial layer in polymer bulk-heterojunction solar cells. Proc Natl Acad Sci 105(8):2783–2787

47. Napari M, Huq TN, Hoye RL, MacManus-Driscoll JL (2021) Nickel oxide thin films grown by chemical deposition techniques: potential and challenges in next-generation rigid and flexible device applications. InfoMat 3(5):536–576

48. Ezugwu AE (2018) Defect-related magnetic properties of nanostructured nickel oxide thin films for solar cell applications. Doctoral dissertation, The University of Western Ontario (Canada)

49. Akl AA, Mahmoud SA, Salman SM (2018) Surface morphology, optical conductivity, localized states, and dielectric constants of sprayed nickel oxide films at different substrate temperatures. Int J Sci Res 7:935

50. Amor MB, Boukhachem A, Boubaker K, Amlouk M (2014) Structural, optical and electrical studies on Mg-doped NiO thin films for sensitivity applications. Mater Sci Semicond Process 27:994–1006

51. Schrade M, Fjeld H, Norby T, Finstad TG (2014) Versatile apparatus for thermoelectric characterization of oxides at high temperatures. Rev Sci Instrum 85(10):103906

52. Beretta D, Bruno P, Lanzani G, Caironi M (2015) Reliable measurement of the Seebeck coefficient of organic and inorganic materials between 260 K and 460 K. Rev Sci Instrum 86(7):075104

53. Abadlia L, Gasser F, Khalouk K, Mayoufi M, Gasser JG (2014) New experimental methodology, setup and LabView program for accurate absolute thermoelectric power and electrical resistivity measurements between 25 and 1600 K: application to pure copper, platinum, tungsten, and nickel at very high temperatures. Rev Sci Instrum 85(9):095121

54. Mili I, Latelli H, Charifi Z, Ghaellab T (2022) A simple formula for calculating the carrier relaxation time. Comput Mater Sci 213:111678

55. Layland WJH, John GH, Harley RT, Glazov MM, Ivchenko EL, Ritchie DA, Farrer I, Shields AJ, Henini M (2007) Enhanced spin-relaxation time due to electron-electron scattering in semiconductor quantum wells. Phys Rev B 75:165309

56. Bub JH, Rudolph J, Natali F, Semond F, Hagele D (2010) Temperature dependence of electron spin relaxation in bulk GaN. Phys Rev B 81:155216

57. Kainz J, Rossler U (2004) Temperature dependence of Dyakonov–Perel spin relaxation in zinc-blende semiconductor quantum structures. Phys Rev B 70:195322

Nayem Md. Reza Shah pursued his Ph.D. from the Department of Mechanical Engineering of Texas Tech University. He worked under the supervision of Dr. Changdong Yeo, in the "Materials and Interface Mechanics Laboratory". He is currently working as a TD Module and Integration Yield Engineer in Intel Corporation, and focused on implementing his knowledge and skill in the semiconductor industry, and to enrich his profile with acquiring and developing newer skills in the related field.

Chang-Dong Yeo is an associate professor in the Department of Mechanical Engineering at Texas Tech University (Texas, USA). He obtained his doctoral degree from the University of Illinois at Urbana-Champaign. Dr. Yeo's group is carrying out a fundamental research on thermo-magneto-electro-mechanical properties of functional materials.

Minyeong Choi obtained his doctoral degree from the Department of Electrical and Computer Engineering at the University of Alabama-Tuscaloosa. He has been working on the electromagnetic properties of ferromagnetic materials and metal oxides through the first principle calculations. He is currently working as a senior engineer in Hyundai Motors, Korea.

Yang-Ki Hong is the E. A. "Larry" Drummond Endowed Chair and Professor of Electrical and Computer Engineering Department at The University of Alabama-Tuscaloosa. Dr. Hong's group is conducting a pioneering research on soft/hard magnetic materials used for electrical vehicles.

Jeong H. You is an associate professor in the department of mechanical engineering at the University of St. Thomas (Minnesota, USA). He obtained his doctoral degree from the University of Illinois at Urbana-Champaign. His research focuses on the electro-mechanical properties of semiconducting materials through the first principle calculations.